Heliyon 10 (2024) e29404

Contents lists available at ScienceDirect

Heliyon

journal homepage: www.cell.com/heliyon

Research article

Qingfei mixture modulates the immune responses in lung cancer through modulating mTOR signaling and gut microbiota-derived short-chain fatty acids

Xiang Qian [a,1], Zhuo Chen [a,1], Xu-Ming Ji [b,1], Yong-Ling Ji [a,1], Jin Wang [a], Yuan-Cai Liu [b], Xia-Cheng Zhou [b], Qing-Lin Li [a], Chang-Yu Li [b,**], Ai-Qin Zhang [a,*]

[a] Zhejiang Cancer Hospital, Zhejiang, China
[b] Zhejiang Chinese Medical University, Zhejiang, China

ARTICLE INFO

Keywords:
Qingfei mixture
Metabonomics
SCFAs
Gut microbiota
Lung cancer

ABSTRACT

Lung cancer ranks among the primary contributors to cancer-related fatalities on a global scale. Multiple research investigations have demonstrated that there exists a dysbiosis within the intestinal bacteria and short-chain fatty acids (SCFAs) is linked with immune responses in lung cancer. Qingfei mixture (QFM) has been widely used in treating lung cancer, yet the active ingredients and roles of the QFM on immune responses by targeting gut microbiota remain to be elucidated. The chemical constituents of QFM were qualitatively examined by UPLC/Q-TOF-MS. Additionally, we evaluated the therapeutic impact of the organic substance QFM on lung cancer, aiming to elucidate its mechanisms for improving the tumor-immune microenvironment. Herein, we constructed a Lewis lung carcinoma (LLC)-bearing mice model with QFM treatment to observe tumor growth and immune cell changes. Then, the feces were collected and a combinatory study using metagenomes, non-targeted metabonomics, and targeted metabonomics of SCFAs was performed. In vitro experiments have been conducted to estimate the roles of acetate and sodium propionate in $CD8^+$ T cells. Furthermore, we treated tumor-bearing mice with QFM, QFM + MHY1485 (an mTOR activator), and QFM + an antibiotic mixture (ABX) to explore the potential therapeutic benefit of regulation of the tumor microenvironment. A total of 96 compounds were obtained from QFM by UPLC/Q-TOF-MS. Besides, the findings demonstrated that QFM exhibited significant efficacy against lung cancer, manifesting in reduced tumor growth and improved immune responses. In investigating its mechanisms, we integrated gut microbiota sequencing and fecal metabolomics, revealing that QFM effectively restored disruptions in gut microbiota and SCFAs in mice with lung cancer. QFM, acetate, or sodium propionate contributed to the up-regulation of IFN-γ, Gzms-B, perforin, IL-17, IL-6, IL-12, TNF-α expressions and decreased HDAC and IL-10 levels in vitro and *in vivo*. Moreover, MHY1485 and ABX weakened the effects of QFM on immunomodulation. Collectively, these results suggest that QFM may facilitate immune

* Corresponding author. Zhejiang Cancer Hospital, No.1 East Banshan Road, Gongshu District, Hangzhou, 310022, China.
** Corresponding author. Zhejiang Chinese Medicine University, No. 548 Binwen Road, Binjiang District, Hangzhou, 310053, Zhejiang, China.
E-mail addresses: 1586710095@163.com (X. Qian), 15757194882@163.com (Z. Chen), jixuming724@163.com (X.-M. Ji), jiyl@zjcc.org.cn (Y.-L. Ji), Wangjin@zjcc.org.cn (J. Wang), 15970114415@163.com (Y.-C. Liu), zxc18868104302@163.com (X.-C. Zhou), qinglin200886@126.com (Q.-L. Li), lm159@sina.com (C.-Y. Li), zhangaq@zjcc.org.cn (A.-Q. Zhang).
[1] Xiang Qian, Zhuo Chen, Xu-Ming Ji, and Ling-Yong Ji contributed equally to this work.

https://doi.org/10.1016/j.heliyon.2024.e29404
Received 4 January 2024; Received in revised form 8 April 2024; Accepted 8 April 2024

responses in the LLC-bearing mice via regulating the gut microbiota-derived SCFAs at least partially through targeting the mTOR signaling pathway.

1. Introduction

One of the most prevalent malignant tumors is lung cancer, which accounts for roughly 11 % of all malignant tumors and approximately 18 % of tumor-related fatalities [1]. In 2023, approximately 103,000 out of the 127,070 lung cancer deaths were directly attributed to cigarette smoking, while an additional 3,560 fatalities were linked to second-hand smoke exposure [2]. Approximately 80 % of instances of lung cancer manifest as non-small cell lung cancer (NSCLC), and due to delayed development of clinical symptoms and insufficient screening techniques, many NSCLC patients receive a diagnosis at an advanced stage [3]. It is challenging to treat NSCLC, and despite the combination of surgery, immunotherapy, chemotherapy, and radiotherapy improving the prognosis for NSCLC, many patients still pass away from the disease due to the recurrence and metastasis [4]. Thus, it is essential to actively investigate the mechanisms and novel therapies of NSCLC.

A significant paradigm change has occurred in lung cancer treatment over the past ten years. Many efficient targeted treatments and immunotherapy have been created as a result of our growing biological understanding of lung cancer. In the realm of NSCLC treatment, the advent of specific antibodies targeting the CTLA4 receptor, PD-L1, and PD-1 has led to unprecedentedly extended survival rates for a portion of these patients [5]. Nonetheless, the majority of individuals continue to experience illness progression while receiving treatment or after stopping the medication. A multi-drug combination therapy that targets T cell activation, co-stimulatory signal activation, tumor microenvironment (TME) modification, and immunological co-inhibitory signal blocking is currently being closely studied [5–7]. Among them, unbalance in the TME, one of the most obvious characteristics of malignancies is inundated with tumor cells, numerous stromal cells consisting of fibroblasts, epithelial cells, and adipocytes, as well as immune cells [8,9]. Additionally, the majority of antitumor cells of the immune system in the TME, known as $CD8^+$ T cells. However, the abundance of immunosuppressive cells or substances within the tumor microenvironment hinders the capability of $CD8^+$ T cells to execute their function [10]. A study by Tu et al. found that the combination of Anti-PD-L1 and anti-CD73 contributes to tumor-infiltrating $CD8^+$ T cells response in EGFR-mutated NSCLC [11]. As is well documented, immunosuppressive regulatory T cells (Tregs), PD-1, and CTLA4 levels were upregulated which ultimately caused the $CD8^+$ T cells exhaustion in TME [12,13]. Therefore, clarifying the regulatory mechanisms and determining the elements that can boost $CD8^+$ T cells in the TME of NSCLC are crucial.

The intestinal flora is made up of millions of intestinal microorganisms, the majority of which are bacteria of all kinds, followed by viruses and certain eukaryotes, with a vital function in maintaining host health [14]. According to studies, there is a connection between gut microbiota and lung cancer. Intestinal flora affects lung cancer's development, invasion, and metastasis as well as the curative effects of chemotherapy and immunotherapy [15,16]. As a result, lung cancer prevention and therapy strategies should consider targeting intestinal flora. Furthermore, SCFAs are the primary metabolites produced by particular intestinal flora, including *Bacteroides*, *Roseburia*, *Bifidobacterium*, *Fecalibacteriu*m, and *Enterobacteria*, following fermentation of dietary fiber and resistant starch [17]. Additionally, it has been demonstrated that the SCFAs produced by the gut microbiota, which are pivotal in preserving cellular homeostasis given that they have an impact on the activity of histone deacetylases (HDACs), which in turn affects cell adhesion, immune cell migration, cytokine secretion, and programmed death of cells [17,18]. Consequently, it may be worthwhile to think about changing the microbiota's structural composition to affect SCFA concentrations in the digestive tract for the purpose of treating or preventing cancer.

Traditional Chinese medicine (TCM), as one of the most important techniques of preventing and treating malignant tumors, aids in the elimination of evil by controlling intestinal flora, enhancing probiotics, reducing dangerous bacteria, and then maintaining flora homeostasis [19,20]. Qingfei mixture (QFM), a hospital preparation based on an experienced recipe for treating medium and late-stage lung cancer, was established by Zhejiang Cancer Hospital (Zhejiang, China). This medicinal mixture is made up of Bulb of Thunberg Fritillary ("Zhe Bei Mu" in Chinese), Stephania tetrandra radix ("Fang Ji" in Chinese), Hedyotis diffusa Herba ("Bai Hua She She Cao" in Chinese), Solanum nigrum L ("Long Kui" in Chinese), Paridis Rhizoma ("Chong Lou" in Chinese), Scutellariae Barbatae Herba ("Ban Zhi Lian" in Chinese), Imperatae Rhizoma ("Bai Mao Gen" in Chinese), Agrimoniae Herba ("Xian He Cao" in Chinese), Prunellae Spica ("Xia Ku Cao" in Chinese), and Scolopendra ("Wu Gong" in Chinese). Modern clinical studies have shown that QFM possesses the ability to improve immunologic function in NSCLC patients by increasing $CD3^+$ and $CD4^+$ T lymphocyte subsets, as well as IgG, IgA, and IgM levels [21,22]. Besides, a large number of contemporary academics have become interested in the makeup of natural medicines and their many active constituents in recent years. However, the active ingredients and biological mechanisms of QFM on intestinal microbiome and SCFAs in the management of NSCLC remain unknown and deserve additional research.

In this paper, we employed UPLC/Q-TOF-MS technology to examine the constituents of QFM. Primarily, the present investigation sought to elaborate the functions of QFM in managing NSCLC. Furthermore, we investigated whether SCFAs or QFM administration could trigger $CD8^+$ T cell responses at least partially through the intestinal flora. Our results indicated that QFM could inhibit tumor growth, restore the intestinal flora, and ameliorate SCFA levels in Lewis lung carcinoma (LLC)-bearing mice. Acetate and propionate or QFM also trigger $CD8^+$ T cell responses in vitro and *in vivo*, respectively. In conclusion, QFM may alleviate $CD8^+$ T cell exhaustion for enhancing immune function through intestinal flora-associated SCFAs in NSCLC.

2. Materials and methods

2.1. Cell culture

Mouse Lewis lung carcinoma-luciferase (LLC-Luc) was purchased from the Cell Resource Center of the Shanghai Academy of Sciences (Shanghai, China). The LLC-Luc cell line was cultured in DMEM (Thermo Fisher Scientific, USA) supplemented with 10 % FBS (Gibco, USA) in an incubator containing 5 % CO_2.

2.2. Preparation of QFM and component analysis of QFM extracts

QFM consists of *Fritillaria thunbergii* Miq (12g), *Stephania tetrandra* S.Moore (16g), *Scleromitrion diffusum* (Willd.) R.J.Wang (16g), *Solanum nigrum* L., 1753 (16g), *Paris yunnanensis* Franch (30.2g), *Scutellaria barbata* D.Don (30.2g), *Imperata cylindrica* (L.) Raeusch (30.2g), *Agrimonia pilosa* Ledeb (15g), *Prunella vulgaris* Linn (30 g), and *Gekko japonicas Dumeril* et Bibron (9 g). In short, all medicinal ingredients were immersed in 6000 mL of distilled water for 30 min and boiled twice for 2 h each. The yield of the aqueous extract was 2.66 g/mL. Following extraction, QFM was stored at 4 °C until further utilization. The aqueous extracts of QFM were identified with a UPLC/Q-TOF-MS system (Waters, UK), and the equipment's conditions were set as Li et al. had suggested [23].

2.3. Imaging with bioluminescence in vivo

Eighteen specific pathogen-free (SPF) male C57BL/6 mice (5–6 weeks of age) weighing 19 g ± 2 g, were obtained from SLAC (Shanghai, China). The mice were maintained in an SPF barrier environment of the Zhejiang Eyoung Biomedical Research and Development laboratory animal research center (SYXK(Zhe)2021-0033, Zhejiang, China). All mice were randomly assigned to three groups (n = 6): control, model, and QFM groups. Applying the dose conversion formula for human-to-animal dosing, based on a human weight of 60 kg and a nude mouse weight of 20 g, (204.6 g × 0.0026)/20 g yields a clinical equivalent daily gavage dose of 26.6 g/kg. With a daily dose volume of 0.2 mL, QFM was prepared at a concentration of 2.66 g/mL. To mimic clinical application, the selected dose of 26.6 g/kg was administered for *in vivo* animal experiments. Then, mice in the model and QFM groups were injected intravenously with 1×10^6 LLC-Luc cells via the tail-vein. In the QFM group, mice were given QFM intragastrically at a dose of 26.6 g/kg daily for 15 days, whereas the mice in the control and model groups received only an equivalent volume of saline for 15 days. For imaging with bioluminescence *in vivo*, mice in the model and QFM groups were injected intraperitoneally with D-Luciferin (200 μL, 15 mg/mL, Yeasen Biotechnology (Shanghai) Co., Ltd, China) and imaged 10–15 min later using the BLT AniView100 In-Vivo Imaging System (Guangzhou Biolight Biotechnology Co., Ltd., China). After that, the intensity of bioluminescence imaging was determined using region of interest (ROI) analysis.

2.4. Assays of cytokine in serum of mice

Mice were euthanized after imaging the bioluminescence *in vivo*, and the blood was obtained and underwent centrifugation at 12,000 rpm at 4 °C for 15 min to isolate the serum. Afterwards, the levels of IFN-γ, IL-6, TNF-α, IL-10 in the serum samples were measured using ELISA with commercial kits (#MM-0182M2, #MM-0132M2, #MM-0163M2, #MM-0176M2, Jiangsu Meimian Industrial Co., Ltd, China).

2.5. Hematoxylin and eosin staining

Mouse tumor tissues were removed, fixed, and embedded in paraffin. Subsequently, the tumor tissues embedded in paraffin were sliced into sections measuring 4 μm in thickness. Next, the sections were stained with hematoxylin and eosin (Sigma, USA). Finally, images were photographed using Eclipse Ci-L microscopy (Nikon, Japan).

2.6. Preparation of $CD8^+$ T cell and flow cytometry analysis

Following the sacrifice of the mice per each group, the spleen was removed, ground, and filtered. Next, the cell filtrate was collected. The sedimentation cells were added with 5 mL red blood cell lysate mix for maintaining 5 min. After centrifugation and discarding the supernatant, the cells were resuspended by PBS solution for further usage. Phenotypes of Tregs in peripheral blood and spleen tissues were conducted with a flow cytometer (BD, USA). Furthermore, $CD8^+$ T cells were purified from spleen mononuclear cells using $CD8^+$ T Cell Biotin-Antibody Cocktail (Miltenyi Biotec, Gladbach, Germany) and MidiMACS™ Separator (Miltenyi Biotec, Gladbach, Germany), as directed by the manufacturer. For the activation and proliferation of $CD8^+$ T cells, the cells were grown in 24-well plates for 48h under anti-CD3 and anti-CD28 antibodies (BD Biosciences, USA) stimulation for further investigation.

2.7. Untargeted metabolomic analysis

The untargeted metabolomic analysis of fecal samples is conducted based on our earlier research [24]. For untargeted metabolomic analysis, we accurately weighed 100 mg of fecal samples in a 2 mL EP tube, added 0.6 mL methanol (−20 °C), and mixed thoroughly by vortexing for 30 s. The samples were then incubated on ice for 5 min and centrifuged at 12000 rpm at 4 °C for 10 min, and the supernatant was filtered through 0.22 μm membrane and added into the detection bottle for LC-MS detection. LC-MS/MS analyses were performed using a Thermo Ultimate 3000 system equipped with an ACQUITY UPLC® HSS T3 (150 × 2.1 mm, 1.8 μm, Waters) column. PCA and OPLS-DA were carried out using the Ropls package. Additionally, differential metabolites with VIP scores exceeding 1 and a

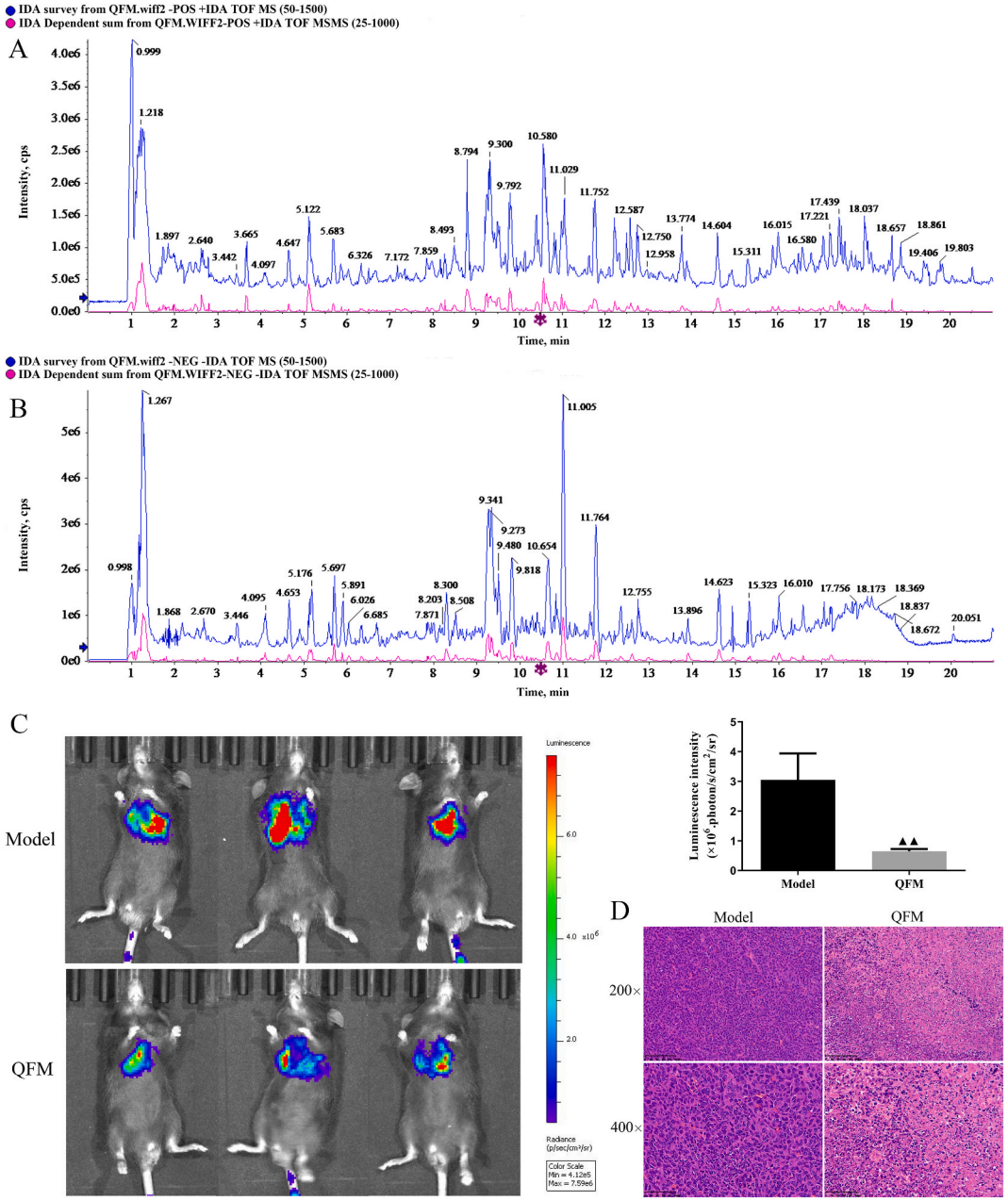

Fig. 1. Component analysis of QFM, and QFM inhibited tumor growth of Lewis lung cancer cells in vivo.
Base peak ion (BPI) chromatogram of chemical compounds of QFM in the positive (A) and the negative ion modes (B) based on UPLC-Q-TOF/MS. (C) Representative *in vivo* images displaying tumor growth in lung derived from mice under tail vein injection of Lewis-Luciferase cells detected via bioluminescence. (D) Representative HE-stained tumor sections from the model and QFM groups.

P-value below 0.05 were visualized on a volcano plot. Finally, the KEGG database was utilized to annotate the functions of metabolites and metabolic pathways.

2.8. Fecal SCFAs analysis

The fecal SCFAs were analyzed as previously reported [25]. Briefly, 50 mg of fecal samples were homogenized with 50 μL of 15 % phosphoric acid and 400 μL of diethyl ether to extract SCFAs. A polar HP-INNOWAX capillary column (30 m*0.25 mm ID*0.5 μm film thickness; Agilent Technologies Inc., USA) was used to detect the levels of SCFAs. The oven program was adopted at an initial temperature of 90 °C, increased to 120 °C at a rate of 10 °C/min, and maintained at 250 °C for 2 min. Peak regions were selected according to the retention time for each SCFA and calculated using MassHunter (Agilent). Subsequently, ROC analysis was performed to evaluate the clinical diagnostic or prognostic potential of the metabolites in QFM-treated lung cancer, with the AUC serving as the assessment metric.

2.9. Fecal microbiota analysis

Bacterial genomic DNA was isolated from each fecal sample using the DNA Stool Kit (Qiagen Bioinformatics Co., Ltd, Hilden, Germany). Metagenomic shotgun sequencing libraries were constructed and sequenced at Suzhou PANOMIX Biomedical Tech Co., LTD (Suzhou, China). The alpha diversity is assessed using three parameters (Simpson, Chao, Shannon), and the beta diversity is assessed using PCoA. Besides, the LEfSe is executed to identify the significantly different species. Moreover, functional annotation of the KEGG orthologs (KOs) was performed using LEfSe analysis. Subsequently, integrating taxa at phylum, genus, and species levels and SCFAs,

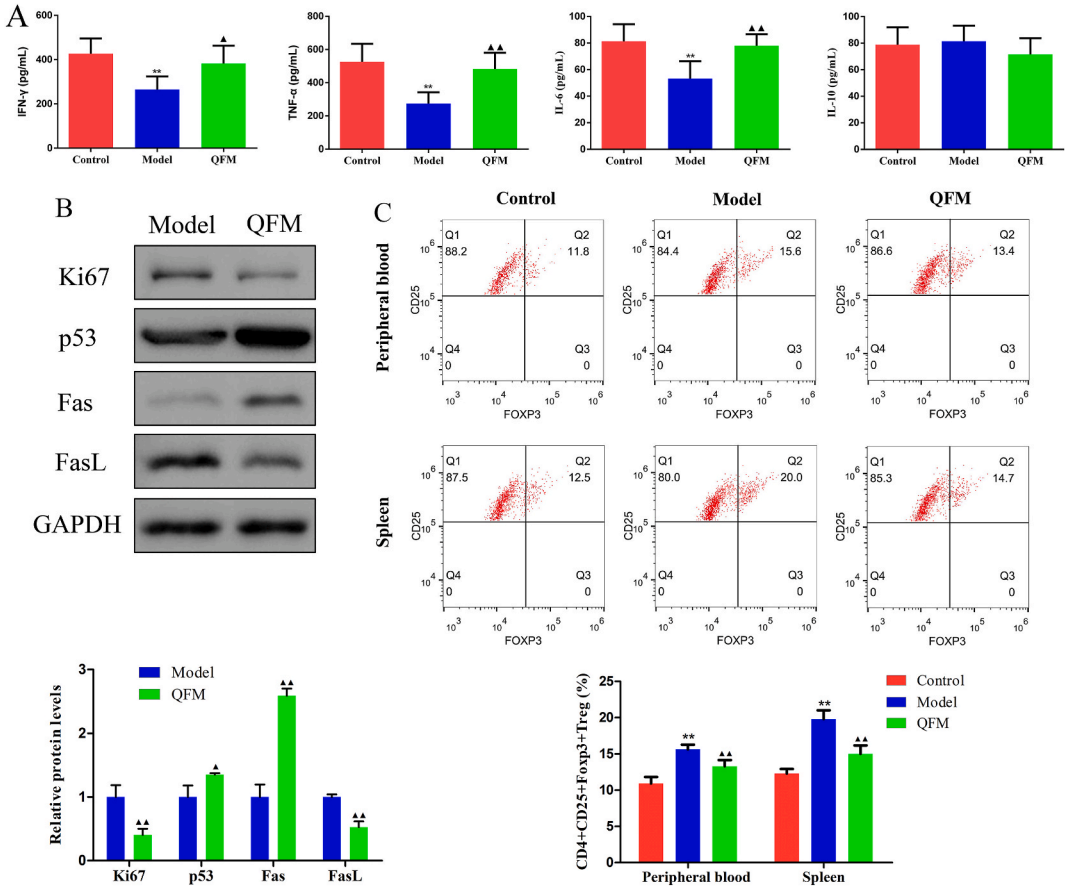

Fig. 2. QFM ameliorated pathogenic factors in mice with Lewis lung cancer. (A) Cytokine expression of IFN-γ, TNF-α, IL-6, and IL-10 in serum of the mice. (B) Protein expression of Ki67, p53, Fas, and FasL in the tumor tissues of the Lewis lung cancer mice by Western blot. (C) The $CD4^+CD25^+Foxp3^+$ Treg cell proportion among $CD4^+$ T cells from peripheral blood and spleen samples of control, model, and QFM groups, measured by flow cytometry. $^{**}P < 0.01$, vs control group; $^{▲}P < 0.05$, $^{▲▲}P < 0.01$, vs model group.

the correlation coefficients between the two components as a heatmap were determined using Spearman analyses using the corrplot package in R.

2.10. Cell viability

The viability of $CD8^+$ T cells was assayed using MTT (BBI Life Sciences). $CD8^+$ T cells were plated in a 96-well plate at a density of 5.0×10^3 cells/well and incubated overnight. After that, the cells were treated with acetate (1 mM, 10 mM, 20 mM) or sodium propionate (0.1 mM, 0.5 mM, 1 mM) at different concentrations for 24h, 48h, and 72h. Next, each well received 20 L of the MTT

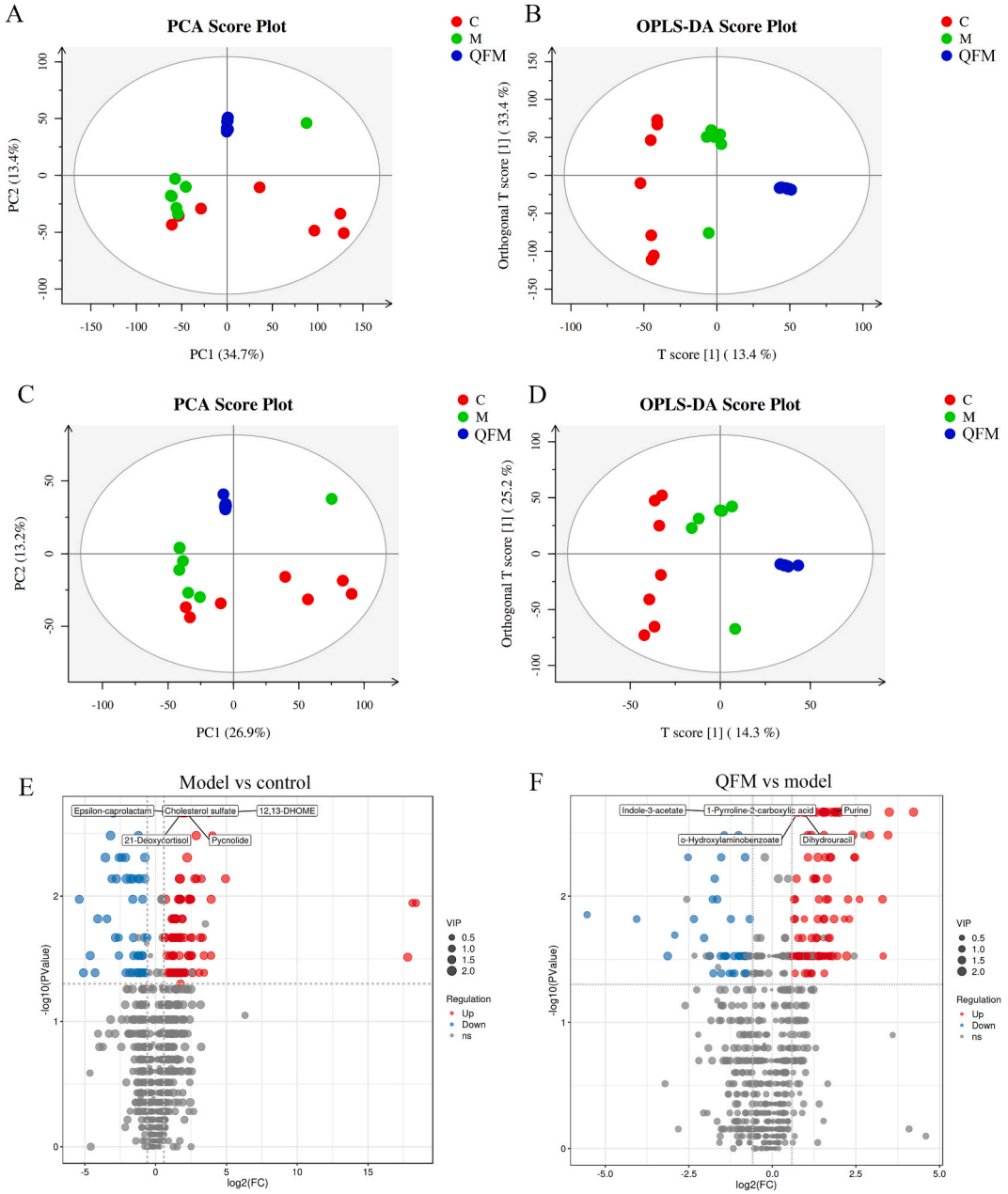

Fig. 3. Metabolic profiles of feces samples in lung mice with QFM treatment. (A) Principal component analysis (PCA) score plot in positive mode. (B) Orthogonal partial least square discriminate analysis (OPLS-DA) score plot in positive mode (M vs C: R2Y = 0.999, Q2Y = 0.627; QFM vs M: R2Y = 0.991, Q2Y = 0.76). (C) PCA score plot in negative mode. (D) OPLS-DA score plot in negative mode (M vs C: R2Y = 0.998, Q2Y = 0.556; QFM vs M: R2Y = 0.997, Q2Y = 0.826). (E) Significant changes in fecal metabolites are shown as a volcano plot showing metabolite changes in the Model (M) and Control (C) groups detected by LC/MS. (F) Significant changes in fecal metabolites are shown as a volcano plot showing metabolite changes in the QFM and Model (M) groups detected by LC/MS.

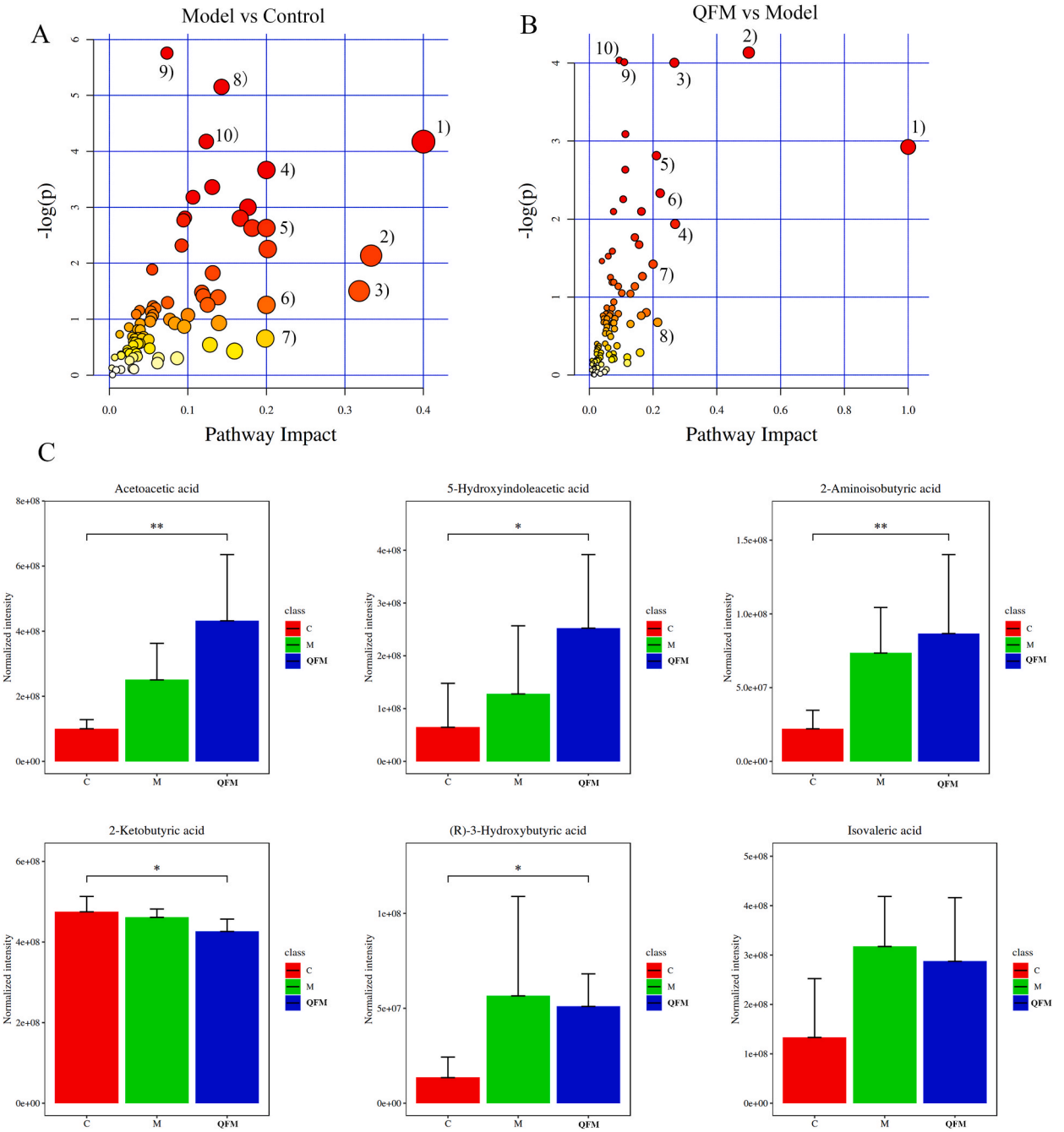

Fig. 4. Metabolic pathway analysis of identified potential metabolites. (A) Overview of metabolic pathway analysis in the Model (M) and Control (C) groups:1) Asthma. 2) Toxoplasmosis. 3) Synthesis and degradation of ketone bodies. 4) Oxidative phosphorylation. 5) D-Arginine and D-ornithine metabolism. 6) Aldosterone-regulated sodium reabsorption. 7) Butanoate metabolism. 8) Mineral absorption. 9) Arachidonic acid metabolism. 10) Lysine degradation. (B) Overview of metabolic pathway analysis in the QFM and Model (M) groups: 1) Basal cell carcinoma. 2) mTOR signaling pathway. 3) D-Arginine and D-ornithine metabolism. 4) Glutathione metabolism. 5) Linoleic acid metabolism. 6) Cholesterol metabolism. 7) PPAR signaling pathway. 8) Ascorbate and aldarate metabolism. 9) Cysteine and methionine metabolism. 10) Arachidonic acid metabolism. (C) Relative abundance of the derivatives of short-chain fatty acids (SCFA). $*P < 0.05$, $**P < 0.01$.

solution (5 mg/mL in PBS) and incubated for 4 h before the culture was stopped and the well's culture supernatant was carefully aspirated. To completely melt the crystal, 150 L of DMSO was added to each well, and the mixture was agitated for 10 min. Ultimately, cell viability was assessed by recording absorbance at 450 nm wavelength utilizing a CMaxPlus microplate reader (Molecular Devices, Germany).

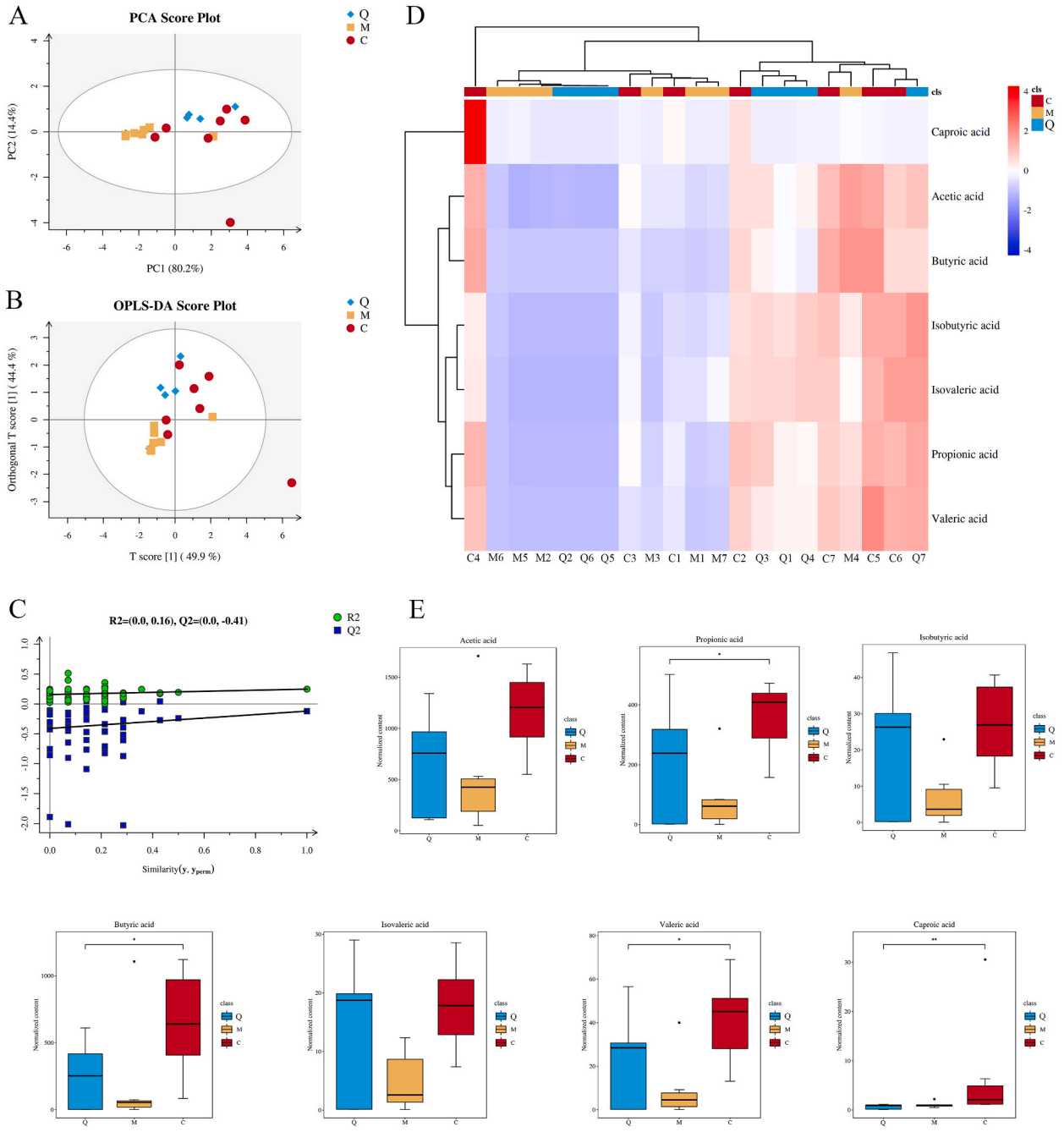

Fig. 5. Determination of fecal SCFA content in QFM-treated mice with lung cancer. (A) PCA score plot (2 principal components, R2X 0.946). (B) OPLS-DA score plot (2 principal components, R2X 0.943, R2Y 0.246, Q2 -0.121). (C) OPLS-DA validation plot intercepts: R2 = (0.0, 0.16), Q2 = (0.0, −0.41). (D) Heatmap visualization of the SCFA in the fecal samples from QFM (Q)-treated lung cancer mice. (E) The content of Acetic acid, Propionic acid, Isobutyric acid, Butyric acid, Isovaleric acid, Valeric acid, and Caproic acid showed using the Box plot. *$P < 0.05$, **$P < 0.01$.

2.11. ELISA and HDAC fluorometric assay

After the cells were treated with acetate (1 mM, 10 mM, 20 mM) or sodium propionate (0.1 mM, 0.5 mM, 1 mM), the level of IFN-γ, Gzms-B, and perforin in the supernatants of the $CD8^+$ T cells was quantified using ELISA kits, according to the manufacturer's instructions. For the HDAC fluorometric assay, the HDAC inhibitory activity of acetate and sodium propionate was measured by the Histone Deacetylase Assay Kit, Fluorometric (AAT Bioquest, Inc., USA). Briefly, after treatment for indicated times, the nucleoprotein of $CD8^+$ T cells was extracted using Nucleoprotein Extraction Kit (Thermo Fisher, USA). Subsequently, different concentrations of acetate or sodium propionate were incubated with the $CD8^+$ T cells lysate and acetylated substrate provided in the kit. The developer solution was added to the aforementioned components after 30 min of incubation, and they were then incubated for an additional 10 min. Ultimately, the fluorescence was detected using a Varioskan LUX multimode plate reader (Thermo Scientific, USA). To assess the HDAC inhibitory activity of acetate and sodium propionate, the HDAC inhibitor trichostatin A at 30 μM was utilized as a reference.

2.12. Western blotting assay

Tumor samples from lung tissues of LLC tumor-bearing mice were homogenized and centrifuged. And, the total protein of acetate- and sodium propionate-treated $CD8^+$ T cells was extracted with RAPI cells lysis buffer (Beijing ComWin Biotech Co., Ltd. China) supplemented with a protease inhibitor cocktail (ComWin Biotech). Then, the protein content was assessed utilizing the BCA kit (Beyotime). An equivalent quantity of protein samples (30 μg) were then separated by 10 % SDS-PAGE and transferred to PVDF (GE Healthcare Life Sciences China, China) membranes and blocked with 5 % bovine serum albumin (BioFRoxx, Germany) in TBST for 2 h. After that, the membranes were exposed to primary antibodies targeting Ki67 (1:1000, AF0198, Affinity Bioscience, USA), p53 (1:1000, AF0879, Affinity), Fas ((1:1000, AF5342, Affinity), FasL (1:1000, AF0157, Affinity), p-mTOR (1:1000, ab109268, Abcam, Cambridge, UK), mTOR (1:1000, ab32028, Abcam), p-p70S6K (1:1000, 9208T, CST, USA), p70S6K (1:2000, 2708T, CST), and GAPDH (1:5000, AF7021, Affinity) at 4 °C overnight. After that, the membranes underwent incubation with anti-rabbit IgG, HRP-linked antibody (1:5000, #7074, CST) or anti-mouse IgG (H + L), biotinylated antibody (1:5000, #14709, CST) for 2 h at room

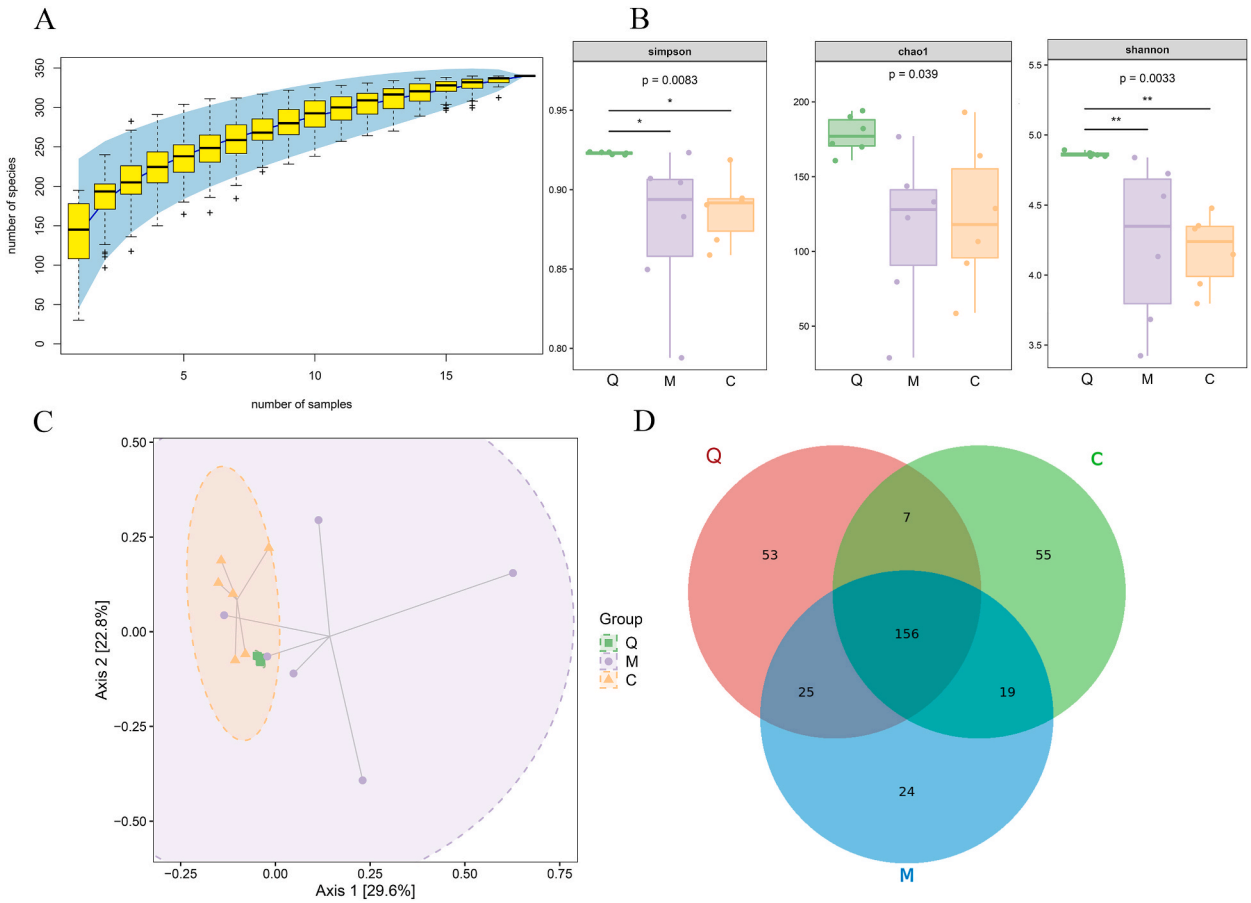

Fig. 6. Altered gut microbiota diversity in QFM-treated mice with lung cancer. (A) Species cumulative box plot of QFM-treated mice gut microbiota. (B) Simpson, Chao1, and Shannon indices were selected to assess the α-diversity of the gut microbiota. (C) PCoA analysis of the gut microbiota. (D) Venn diagram concisely illustrated the operational taxonomic units (OTU) distribution among the C, M, and QFM (Q) groups.

Fig. 7. Distribution of gut microbiota in QFM-treated mice with lung cancer. Taxonomic summary of the gut microbiota in QFM (Q), M, and C groups at the phylum level (A, only top 17 shown), the genus level (B, only top 20 displayed), and the species level (C, only top 20 highlighted). (D) Cladogram generated by the Linear discriminant analysis (LDA) Effect Size (LEfSe) analysis showing discriminative taxa in the feces from the QFM (Q), M, and C groups. (E) Histogram of the LDA scores for different abundant genera in the QFM (Q), M, and C groups. Purple, enriched in QFM (Q) group; red, enriched in the M group; green, enriched in the C group.

temperature. In the end, the proteins were detected utilizing an ECL chemiluminescence kit (Beyotime, China), followed by exposure with the CLiNX GenoSens2000 Imaging System (Shanghai CLiNX Co., LTD, China), and quantified by using ImagePro Plus software.

2.13. Xenograft model

Male C57BL/6 mice (n, 30; Qualified number: 20170005073685) within 5-weeks-old were purchased from SLAC Co., Ltd. LLC cells (2×10^6 in 200 μL of PBS) were injected subcutaneously into the flanks of each mouse. As the subcutaneous tumors reached a size of about 100 mm^3, mice were randomly divided into five groups: Mice in the model group were administrated physiological saline, sodium propionate group (200 mg/kg, i.g., twice daily; Shanghai Yuanye Biotechnology Co., LTD, China), QFM group (26.6 g/kg, i.g., each day), QFM + MHY1485 [26.6 g/kg, i.g., each day+10 mg/kg, i.p., an mTOR activator (MedChemExpress, China), each day] group, and QFM + antibiotic mixture (ABX) group [(26.6 g/kg, i.g., each day+250 μl of ABX, i.g., twice daily; Macklin, China]. The

Fig. 8. Functional characterization of gut microbiota in QFM-treated mice with lung cancer. (A) Functional annotation of the Kyoto Encyclopedia of Genes and Genomes (KEGG) orthologs (KOs) is shown as 50 categories of KEGG metabolism pathways. The right and left vertical axis represents the primary and secondary classification information of KEGG metabolism pathways, respectively. (B) Differentially abundant pathways were identified using LEfSe for KOs in all microbial communities among the QFM (Q), M, and C groups. (C) Partial least squares-discriminant analysis (PLS-DA) analysis of the KEGG functional pathways shows the intra-group similarity and inter-group difference among the QFM (Q), M, and C groups. The H(Q) group was shown in yellow, the M group was shown in gray, and the C group was shown in blue, n = 6 per group.

volume of tumor xenografts was measured every three days by vernier calipers and calculated using the following formula: volume (mm^3) = 0.5 × $width^2$ × length. After 15 days of treatment, the mice were anesthetized to collect the blood samples and euthanized using cervical dislocation to harvest their tumors and thymus tissues. The thymus tissues and blood samples were then used for evaluating the levels of HDAC, IL-17, IL-6, IL-10, IL-12, IFN-γ, and TNF-α with commercial kits. Besides, the thymus tissues and tumors were used for immunohistochemical analysis.

2.14. Immunohistochemistry (IHC) assay

Thymus tissues and tumor samples were fixed in 4 % paraformaldehyde, embedded in paraffin, and sectioned. The methodology for IHC has been described previously [26]. The tissue sections were cultured with primary antibodies containing rabbit anti-mouse CD4 (1:1000, ab183685, Abcam) and CD8 (1:2000, ab209775, Abcam) at 4 °C overnight and then treated with an HRP-conjugated secondary antibody. Finally, images were acquired using an AE2000 light microscope system (Motic, Germany).

2.15. Statistical analysis

Data were shown as means± standard deviations (SD). Differences between the two groups were assessed using 2-tailed Student's t-tests. A significance level of $P < 0.05$ was employed for statistical analysis.

3. Results

3.1. QFM-induced inhibition of tumor growth and anti-tumor immunity in mice

To survey the overall fragmentation profile of QFM, the aqueous extract was subjected to UPLC-Q/TOF-MS examination. The entirety of the ion chromatography of QFM was shown in positive and negative ion modes (Fig. 1A–B). According to the analysis's findings, the partial ingredients could be also found in the positive and negative ion modes. Fifty-six chemical ingredients were identified under positive ion mode (Table S1) and fifty-seven chemical ingredients under negative ion mode (Table S2). After removing duplicate items, a total of 96 chemical ingredients were identified from QFM.

To identify the potential anti-tumor effect of QFM on tumor growth and migration ability in lung cancer, we treated LLC-luc cells tumor-bearing mice with QFM (26.6 g/kg). The outcomes revealed that the growth of the luminescence signals of LLC-luc cells transplanted mice treated with QFM was notably reduced than that observed in mice from the model group. (Fig. 1C). We also found that the QFM group possessed the distinct ablation of tumor cells when compared to the model group (Fig. 1D). Additionally, immune cytokines in the serum samples of the tumor-bearing mice were measured to estimate the immunomodulation effects of QFM. As illustrated in Fig. 2A, QFM observably increased the content of IFN-γ, IL-6, TNF-α, whereas there was no notable variance in IL-10 levels. Furthermore, the protein expression of Ki67, p53, and the apoptosis-related proteins Fas and FasL, was detected by Western blot. Compared with the model, treatment with QFM decreased the expression of Ki67 and FasL, while promoting the increase of p53 and Fas levels in tumor tissues (Fig. 2B). More importantly, we also detected the number of $CD4^+CD25^+Foxp3^+$ Treg cells in the peripheral blood and spleen tissues of mice by flow cytometry. The results showed that FOXP3-positive Treg cells in the peripheral blood and spleen tissues of mice significantly decreased when compared with the model group (Fig. 2C). Taken together, these findings indicated that QFM might contribute to rectifying the tumor immune microenvironment for releasing its anti-tumor effects in lung cancer.

3.2. Fecal untargeted metabolomics of QFM-treated tumor-bearing mice

We conducted PCA and OPLS-DA analyses to discern the variations in fecal metabolites across the control, model, and QFM groups. The results found that the metabolic patterns of the three groups indicated favorable separation in positive mode (Fig. 3A–B) and negative mode (Fig. 3C–D), respectively, suggesting that lung cancer and QFM could result in changes in biomarkers in feces. Following the examination, we identified a total of 116 differentially expressed metabolites between model and control groups with VIP>1 and $P < 0.05$. Among these, 79 were found to be up-regulated, while 37 were down-regulated (Fig. 3E). Similarly, a total of 109 differentially expressed metabolites between QFM and model groups were plotted in Fig. 3F, of which 75 were upregulated and 34 were downregulated. And, more details about these differentially expressed metabolites are shown in Table S3. In the current study, MetaboAnalyst was adopted to inquire about the biochemical pathways based on the metabolomics data, and 10 metabolic pathways were selected as the most important metabolic pathways associated with Asthma, Toxoplasmosis, Synthesis and degradation of ketone bodies, Oxidative phosphorylation, D-Arginine and D-ornithine metabolism, Aldosterone-regulated sodium reabsorption, Butanoate metabolism, Mineral absorption, Arachidonic acid metabolism, and Lysine degradation between model and control groups (Fig. 4A). In addition, top enriched signaling pathways in QFM and model groups included basal cell carcinoma, mTOR signaling pathway, D-Arginine and D-ornithine metabolism, Glutathione metabolism, Linoleic acid metabolism, Cholesterol metabolism, PPAR signaling pathway, and Arachidonic acid metabolism (Fig. 4B). A large number of researches have documented that SCFAs are involved in cancer progression [27,28]. We also focused on SCFAs or their derivatives in Lung cancer mice, such as acetoacetic acid, 5-Hydroxyindoleacetic acid, 2-Aminoisobutyric acid, 2-ketobutyric acid, (R)-3-Hydroxybutyric acid, and isovaleric acid, which exhibited higher concentrations in QFM group than in control group (Fig. 4C). As mentioned above, altered gut metabolism QFM-treated LLC-luc cells tumor-bearing mice may be related to the gut SCFAs undulations.

3.3. Fecal SCFAs analysis of QFM-treated tumor-bearing mice

To more accurately assess the impact of QFM on SCFAs in mice with lung cancer, the targeted metabolomics of SCFAs was performed in stool samples again. Using PCA and OPLS-DA (Fig. 5A–B), obvious differences in feces SCFAs existed among the three groups. Besides, the permutation test for OPLS-DA indicated that the Q2 regression line had a negative intercept. Moreover, the Q2 values on the left were lower than the original points on the right, suggesting that the OPLS-DA model in this paper is acceptable (Fig. 5C). Finally, 7 SCFAs including Acetic acid, Propionic acid, Isobutyric acid, Butyric acid, Isovaleric acid, Valeric acid, and Caproic acid were shown in the heatmap (Fig. 5D). The content levels of SCFAs were significantly decreased in model group. Besides, we also observed a significant increase in SCFAs levels in QFM treatment group, as illustrated in Fig. 5E.

To determine the clinical value of SCFAs between the three groups, the ROC curve analysis was carried out. The results indicated Acetic acid (sensitivity: 85.7 %, specificity: 100 %, AUC = 0.857), Propionic acid (sensitivity: 85.7 %, specificity: 100 %, AUC = 0.959), Isobutyric acid (sensitivity: 85.7 %, specificity: 85.7 %, AUC = 0.918), Butyric acid (sensitivity: 85.7 %, specificity: 100 %, AUC = 0.888), Isovaleric acid (sensitivity: 85.7 %, specificity: 85.7 %, AUC = 0.959), Valeric acid (sensitivity: 85.7 %, specificity: 100 %, AUC = 0.959), and Caproic acid (sensitivity: 85.7 %, specificity: 100 %, AUC = 0.929) between model group and control group could become feces biomarkers to diagnose lung cancer (Fig. S1). Furthermore, the ROC analysis also showed that Acetic acid

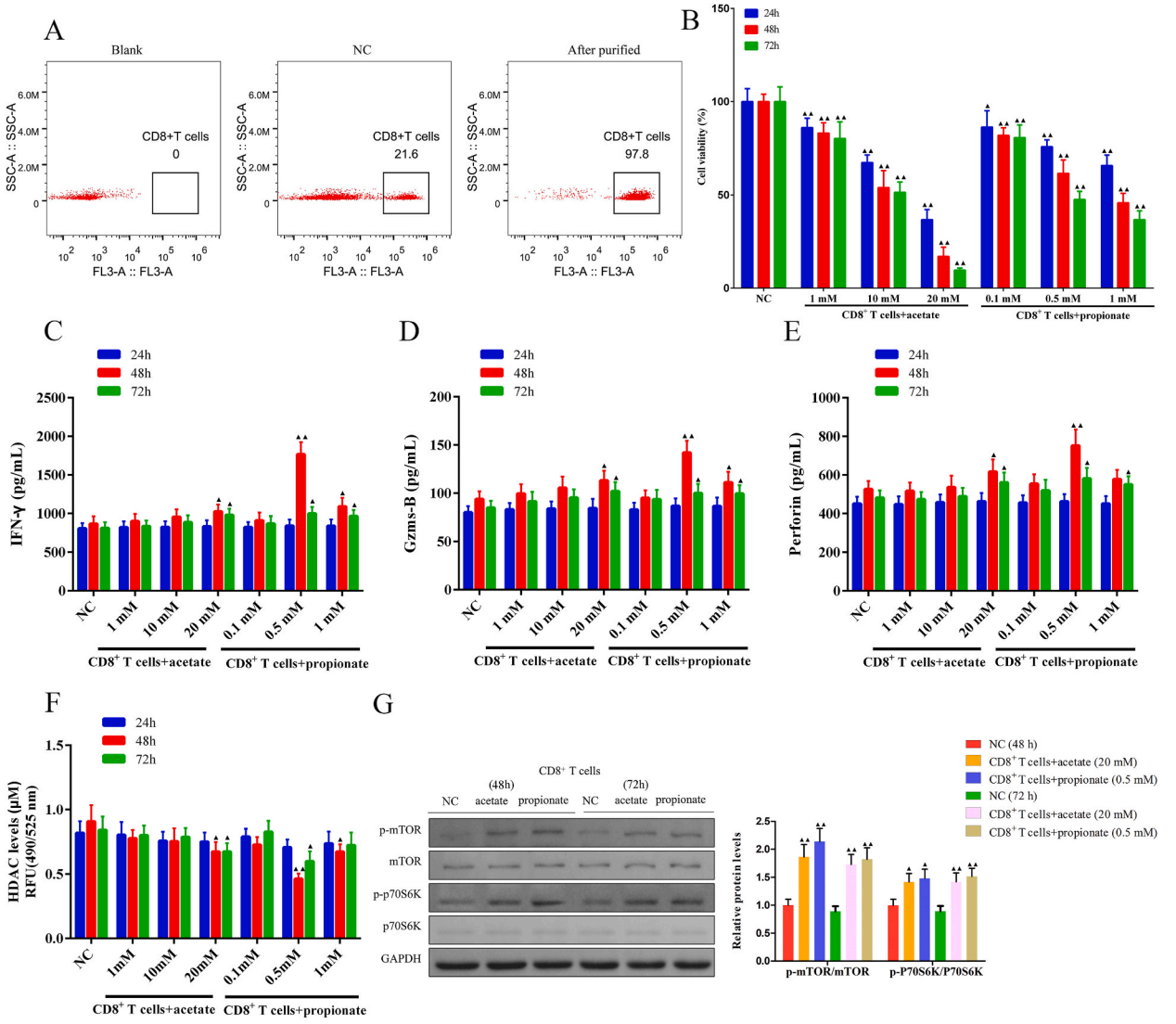

Fig. 9. Effect of acetate and propionate on immune signatures in CD8$^+$ T cells. (A) Purification of CD8$^+$ T cells was performed by flow cytometry using the set gating strategy. (B) Cell viability assays for CD8$^+$ T cells with different concentrations of acetate and propionate treatment for 24h, 48h, and 72h. (C–F) The secretion of IFN-γ, Gzms-B, Perforin, and HDAC in the culture supernatant by CD8$^+$ T cells treated with acetate and propionate was analyzed by ELISA and HDAC fluorometric assays, respectively. (G) Protein expression levels of mTOR/p70S6K pathway-associated targets in acetate and propionate-treated CD8$^+$ T cells were examined by Western blotting. $^{\blacktriangle}P < 0.05$, $^{\blacktriangle\blacktriangle}P < 0.01$, vs NC group.

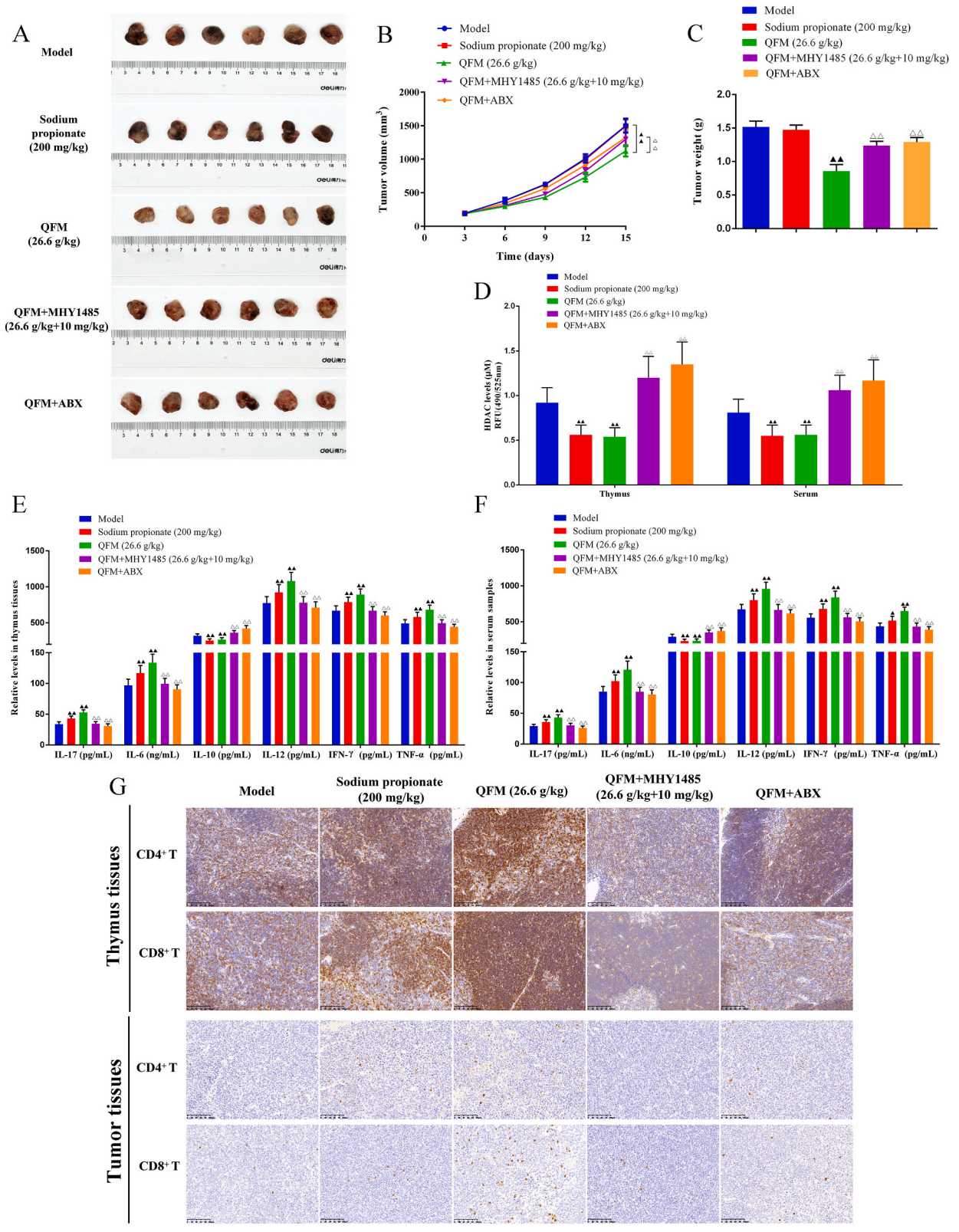

(caption on next page)

Fig. 10. QFM inhibited the cancer growth and improved the immunosuppressive environment in vivo. (A) Representative images of xenograft tumors formed by Lewis lung carcinoma cells in the C57BL/6 mice treated with sodium propionate, QFM, QFM + MHY1485 (an mTOR activator), QFM + an antibiotic mixture (ABX). (B) Tumor volume and (C) the average tumor weight of mice subcutaneous xenograft after QFM treatment at day 15. (D–F) HDAC, IL-17, IL-6, IL-10, IL-12, IFN-γ, and TNF-α levels in thymus tissues and serum samples of C57BL/6 mice were highlighted using commercial kits. (G) QFM treatment promoted the cell proliferation of $CD4^+$ and $CD8^+$ T lymphocytes in thymus tissues, as well as the infiltration of $CD4^+$ and $CD8^+$ T lymphocytes in subcutaneous xenograft, as displayed by immunohistochemical staining. Scale bar, 100 μm $^{\blacktriangle}P < 0.05$, $^{\blacktriangle\blacktriangle}P < 0.01$, vs model group. $^{\triangle\triangle}P < 0.01$, vs QFM group.

(sensitivity: 57.1 %, specificity: 85.7 %, AUC = 0.612), Propionic acid (sensitivity: 57.1 %, specificity: 85.7 %, AUC = 0.643), Isobutyric acid (sensitivity: 57.1 %, specificity: 100 %, AUC = 0.571), Butyric acid (sensitivity: 57.1 %, specificity: 85.7 %, AUC = 0.531), Isovaleric acid (sensitivity: 57.1 %, specificity: 100 %, AUC = 0.684), Valeric acid (sensitivity: 57.1 %, specificity: 85.7 %, AUC = 0.592), and Caproic acid (sensitivity: 42.9 %, specificity: 100 %, AUC = 0.592) could be developed as stool biomarkers for evaluating therapeutic potentiality of QFM in lung cancer to a certain extent (Fig. S2). As a result, these findings demonstrate that SCFAs may be significantly related to the efficacy features of QFM on intestinal regulation in tumor-bearing mice.

3.4. Fecal microbiological analysis of QFM-treated tumor-bearing mice

As seen in the species cumulative box plot (Fig. 6A), since the number of test samples increased, the curves got flatter. Doing so meant that the number of samples in this investigation had met the basic detection and sucient levels, allowing the species richness to be completely represented. Besides, the α-diversity indexes, including the Simpson index, Chao index, and Shannon index, are usually used for assessing community richness and diversity. As depicted in Fig. 6B, there was a notable variance in microbial richness determined between the QFM group and the model group. To identify the gut microbiota structure between the samples, we also performed PCoA analysis. As shown in Fig. 6C, the confidence ellipses of mice in QFM and model groups have been mostly separated, while the confidence ellipses of QFM and control groups have been completely overlapped. In addition, a total of 156 OTUs were shared among the three groups. A total of 53, 55, and 24 unique OTUs were reserved in QFM, control, and model groups, respectively (Fig. 6D). The above finding suggested that the quantity of gut-specific OTUs in QFM group was significantly greater than that in model group, indicating, thereby that the structure and diversity the of intestinal microbial community was ameliorated by QFM treatment, even gradually similar to the control group.

To go deeper into the characteristics of the intestinal microbiota linked to QFM, we annotated the OTUs using QIIME software. The composition of gut microbiome is illustrated in the stacked bar charts (Fig. 7A–C). At the phylum level, *Proteobacteria*, *Chiamydiae*, *Verrucomicrobia*, *Firmicutes*, and *Bacteroidetes* possessed a substantial portion; *Bacteroidetes* and *Chiamydiae* were increased in QFM group mice when compared with model mice, while *Proteobacteria* and *Firmicutes* were decreased. A significant augmentation in *Bacteroides*, *Paramuribaculum*, *Akkermansia*, *Chlamydia*, *Oscillibacter*, and *Fibrobacter* at the genus level was observed in the QFM group in comparison with the model group. Beside, we found that the reduced abundance of *Muribaculaceae bacterium Isolate-037 (Harlan)*, *Muribaculaceae bacterium Isolate-007 (NCI)*, *Muribaculaceae bacterium Isolate-080 (Janvier)* were observed in model mice. After treatment with QFM, the structure of bacteria in model mice tended to control mice. Furthermore, the LEfSe analysis was employed to discover bacterial taxa whose relative abundance differed significantly between the control, QFM, and model mice. As shown in Fig. 7D, an evolutionary tree diagram depicting the sequences of the three groups, with each circle denoting the taxonomic level ranging from the phylum to species. The results of LDA analysis showed that LDA values of 101 different bacterial genera were greater than 2.43 (LDA ≥2.43, $P < 0.05$). As shown in Fig. 7E, f_*Muribaculaceae*, f_*Lactobacillaceae*, g_*Lactobacillus*, and s_*Lactobacillus_murinus* were found to be more abundant in the control group. The QFM group demonstrated significant enrichment in f_*Bacteroidaceae*, g_*Bacteroides*, g_*Odcillibacter*, and f_*Oscillospiraceae.* Also, the majority of the population in the model group included c_*Gammaproteobacteria*, o_*Deferribacterales*, and p_*Deferribacteres,* they may also be investigated further as predictive factors for making contributions to group differences.

(KOs) is a taxonomic system of proteins whereby a proteins with remarkably similar sequences and features that follow a common pathway can be clustered together [29]. To further elucidate the functional modules of the fecal microbiome between the three groups, we annotated the multifarious KOs to relevant pathways in KEGG database. As shown in Fig. 8A, a total of 50 KOs were screened in these three groups. To sort out variant functional metabolism pathways, Lefse analysis of KEGG functional profiles was conducted. As a result, we found that Biotin metabolism, Penicillin and cephalosporin biosynthesis, Fructose and mannose metabolism were enriched in the control group, while Carbohydrate metabolism, Branched dibasic acid metabolism, and Thiamine metabolis were enriched in the QFM group, as well as Cell cycle Caulobacter, Nitrotoluene degradation, and Lysine degradation were involved in model group (Fig. 8B). Additionally, there was a clear separation of KOs as revealed by the PLS-DA model among the three groups (Fig. 8C). According to existing studies, carbohydrate metabolism and Branched dibasic acid metabolism are involved in the production of SCFAs and nitrogen, respectively [30,31], while Thiamine metabolis is associated with immune function in cancer [32]. Thus, these results indicate that the functional profiles of intestinal tract bacteria in QFM-treated tumor-bearing mice may suggest the variance in SCFAs metabolism and immune-enhanced state.

3.5. Correlational analysis between gut microbiota and SCFAs

To delve deeper into the intimate connection between bacterial genera and lung cancer, we explored the correlation between gut microbiota and SCFAs. Unexpectedly, no significant correlations were observed between gut microbiota and SCFAs at a phylum level

(Fig. S3A). As shown in Fig. S3B, caproic acid showed a negative correlation with the *Acinetobacter*, *Dubosiella*, *Butyricimonas* and a positive correlation with Klebsiella, Shewanella, Turicibacter, Sphingobacterium; also, isobutyric acid, isovaleric acid, and valeric acid showed a positive correlation with Salmonella at the genus level (Fig. S3B). Moreover, associations between the gut microbiota and SCFAs at species level were identified in the correlation analysis, as illustrated in Fig. S3C.

3.6. Acetate and sodium propionate increased production of immune-related cytokines in $CD8^+$ T cells

To investigate the underlying effects of acetate and sodium propionate, we performed CCK-8, ELISA, HDAC fluorometric, and Western blot analyses of $CD8^+$ T cells, sorted from the spleen tissues of mice by flow cytometry (Fig. 9A). Unexpectedly, the cell viability of $CD8^+$ T cells was markedly inhibited after different concentrations of acetate and sodium propionate treatment (Fig. 9B). Furthermore, the ELISA and HDAC fluorometric assays were used to determine the effects of acetate and sodium propionate on the production of immune-related cytokines in $CD8^+$ T cells. The results showed that acetate and sodium propionate significantly promoted the generation of IFN-γ, Gzms-B, and perforin, while in suppressed the HDAC levels in $CD8^+$ T cells, of which 20 mM of acetate and 0.5 mM of sodium propionate displayed a most significant effect at 48h (Fig. 9C–F). The seemingly contradictory results of SCFAs induced inhibition $CD8^+$ T cells proliferation and increased cytokine secretion should be discussed. Hence, we can infer that acetate and sodium propionate may have restored the diminished responsiveness of $CD8^+$ T cells by enhancing cytokine production, while not influencing cell proliferation. Recent research illuminated that mTOR signaling is associated with the regulation of the proliferation, apoptosis, and metabolism of $CD8^+$ T cells [33,34]. After specific acetate and sodium propionate treatment for 48 or 72h, we also found significantly increased p-mTOR and p-p70S6K protein expression levels in $CD8^+$ T cells (Fig. 9G). Collectively, these findings indicate that SCFAs acetate and sodium propionate may be attributed to the increase of immune-related cytokines in $CD8^+$ T cells via the activation of the mTOR/p70S6K axis.

3.7. Antitumor efficacy of QFM and ABX combination therapy in vivo

A xenograft model was initiated in C57BL/6 mice to assess the impact of sodium propionate, QFM, and the combination of QFM with MHY1485 or ABX on tumors *in vivo*. After QFM treatment of C57BL/6 mice for 15 d, the tumor volume and tumor weight were significantly decreased, while there were no statistically substantial variances in the sodium propionate group compared to the model group (Fig. 10A–C). The results of ELISA and HDAC fluorometric assays demonstrated that sodium propionate and QFM treatment markedly increased the expression levels of IL-17, IL-6, IL-12, IFN-γ, and TNF-α, meanwhile decreasing expression of HDAC, IL-10, and MHY1485 or ABX could reverse these effects in thymus tissues and serum samples (Fig. 10A–F). The same trend was discovered in the proliferation of $CD4^+$ and $CD8^+$ T cells in thymus tissues and carcinoma tissues, as evidenced by IHC analysis (Fig. 10G). Overall, these results revealed that the effect of the QFM-ameliorated tumor immune environment may be working by decreasing the mTOR signaling and maintaining the balance of the intestinal microflora.

4. Discussion

Immune escape is a major characteristic of many cancers, including NSCLC [35]. Cancer cells frequently avoid immune detection by repressing the manufacturing of IFN-γ and $CD8^+$ T-cell proliferation, as well as elevating circulating $CD4^+CD25^+Foxp3^+$ regulatory T (Treg) cell-mediated immunosuppression [36,37]. TCM as adjuvant therapy is extensively employed in NSCLC patients for improving cellular immune function [20]. Within this investigation, a total of 96 ingredients were identified in the QFM. Among them, as the pharmacodynamics material basis of QFM, amino acids, phenylpropanoids, polysaccharides, nucleosides, alkaloids, and flavonoids are believed to confer beneficial properties against lung cancer through various cellular aspects. Additionally, we found that the QFM possesses its antitumor potential through its immune-modulating activity. Also, it was found that the QFM could inhibit tumor growth in LLC-luc tumor-bearing mice. After treatment by the QFM, it also resulted in modifications in the upregulation of the TNF-α, IFN-γ, and IL-6, as well as the upregulation of p53, Fas, and FasL protein levels. Furthermore, it was interesting to bring up the downregulation of the proportion of $CD4^+CD25^+Foxp3^+$ Treg cells in the peripheral blood and spleens of mice in the QFM group. In light of the information presented above, it could be deduced that the antitumor contribution of the QFM is strongly connected to immunomodulation. However, the precise mechanism associated with the procedure was mysterious.

Metabolic profiling is springing up as an effective method for detecting various tumors. In the current study, we performed fecal untargeted metabolomic analysis and SCFAs analysis to uncover endogenous biomarkers and potential mechanisms in QFM-treated LLC-luc tumor-bearing mice. Among the dramatically altered metabolites, what drew our interest was that several SCFAs derivatives were drastically altered in the fecal samples from QFM-treated mice. The most obvious outcome of our research was that the main metabolites were linked to the mTOR signaling pathway, D-Arginine and D-ornithine metabolism, Glutathione metabolism, Linoleic acid metabolism, Cholesterol metabolism, PPAR signaling pathway, and Arachidonic acid metabolism between QFM and model group. Among them, it is documented in the literature that hyperactivation of mTOR is involved in cell growth, proliferation, drug resistance, and metabolism in lung cancer [38,39]. Yan et al. documented a notable elevation in linoleic acid levels among NSCLC patients following administration of PD-1 and PD-L1 inhibitors [40]. In addition, untargeted metabolomics analysis was conducted on SCFAs, we found that the relative levels of Propionic acid, Acetic acid, Valeric acid, Butyric acid, Isobutyric acid, and Isovaleric acid were significantly increased by QFM treatment, suggesting that QFM could regulate the metabolism of the intestinal microflora in lung cancer mice. Furthermore, ROC analysis demonstrated that SCFAs were able to predict prognosis effectively in QFM-treated LLC-luc tumor-bearing mice. All results indicated that SCFAs in feces would be a potential biomarker for the QFM treatment in NSCLC.

The ethology or progression of NSCLC has indeed been associated with a variety of variables, including gut microflora [41]. More importantly, recent studies have revealed that SCFAs can be significantly affected by the composition of the gut microbiome [18,42]. Moreover, we utilized metagenomic sequencing to determine whether the composition of stool microorganisms had a relationship with SCFAs in QFM-treated mice. In addition, the species cumulative box plot suggested that the number of samples was sufficient for the analysis. With the Simpson, Chao1, Shannon index, and PCoA analysis, the α and β diversity showed a significant difference among the three groups. Furthermore, commensal bacteria such as *Akkermansia muciniphila*, *Bacteroides*, *Paramuribaculum*, and *Fibrobacter* at the genus level were found to be more abundant in the QFM group than in model mice. In particular, *Akkermansia muciniphila*, a microbiota recognized for mucin degradation, has been reported to be related to the clinical response of PD-1 blockade in advanced NSCLC patients [43]. LEfSe analysis further identified *Bacteroides* at the genus level as one of the biomarkers for QFM treatment. We also identified that carbohydrate metabolism and branched dibasic acid metabolism were the top significantly enriched metabolic pathways in the QFM-challenged mice. SCFAs derived from carbohydrate metabolism processes are essential for gut homeostasis maintenance [44]. In general, a gain of SCFAs in QFM-treated mice by improving gut microbiota particularly for *Akkermansia muciniphila* at least in part contributes to the inhibition of tumor progression.

As we know, SCFAs are the primary metabolites produced during carbohydrate and protein catabolism [45] and generated by *Akkermansia muciniphila* and *Faecalibacterium prausnitzii* [46]. The SCFAs, acetate and propionate have been reported to affect $CD8^+$ T cell responses at the molecular level [47,48]. Furthermore, because of their low molecular mass, SCFAs might penetrate the nucleus of cancer cells, thereby inhibiting histone deacetylase activity and exerting a direct anti-cancer influence [49]. Similarly, we found that acetate and propionate increased the levels of IFN-γ, Gzms-B, perforin and decreased the HDAC levels in $CD8^+$ T cells, as accompanied by an increase of p-mTOR and p-p70S6K protein expressions, suggesting that there are SCFAs-independent mechanisms underlying the cellular function of $CD8^+$ T cells. Meanwhile, we demonstrate that QFM inhibited tumor growth in subcutaneous xenograft tumor mice and promoted IL-17, IL-12, IL-6, TNF-α, IFN-γ expressions and decreased HDAC and IL-10 levels in thymus tissues and serum samples. Moreover, we discovered that QFM encouraged the growth of $CD4^+$ and $CD8^+$ T cells in thymus tissues and tumor tissues of mice, while MHY1485 and ABX reversed the immunomodulatory effects of QFM, implying that QFM may aid in the maintenance of the intestinal microbiota homeostasis to ameliorate the tumor-immune microenvironment by targeting the mTOR signaling.

5. Conclusion

In summary, our findings indicated that the Qingfei mixture inhibited the immune environment of tumor growth *in vivo* via upregulating SCFAs and $CD8^+$ T cells by altering the gut microbiota. Moreover, initial research findings indicated that the Qingfei mixture's therapeutic effects on lung cancer might operate through the mTOR signaling pathway, laying the groundwork for a more in-depth investigation of the mechanism of Qingfei mixture in lung cancer. These findings imply that the Qingfei mixture has the prospects of clinical application to be used as an anti-lung cancer supplement in NSCLC patients and would lead to the development of a potential therapeutic strategy against lung cancer. On the other side, further experimental evaluation should be needed to validate this scientific theory, including the fecal microbiota transplantation (FMT) experiment.

Funding

This project was backed by the Natural Science Foundation of China (No. 81973771).

Ethics approval

All procedures of the animal study were approved by the Animal Experimentation Ethics Committee of Zhejiang Eyong Pharmaceutical Research and Development Center (No. EYOUNG-202103110-01).

Data availability statement

The datasets used and/or analyzed during the present study are accessible from the corresponding author upon reasonable request.

CRediT authorship contribution statement

Xiang Qian: Writing – review & editing, Writing – original draft, Methodology, Investigation, Conceptualization. **Zhuo Chen:** Writing – original draft, Investigation, Conceptualization. **Xu-Ming Ji:** Writing – review & editing, Supervision, Conceptualization. **Yong-Ling Ji:** Methodology, Investigation, Data curation. **Jin Wang:** Investigation, Formal analysis. **Yuan-Cai Liu:** Investigation, Formal analysis. **Xia-Cheng Zhou:** Investigation, Formal analysis. **Qing-Lin Li:** Writing – review & editing, Project administration, Conceptualization. **Chang-Yu Li:** Writing – review & editing, Project administration, Conceptualization. **Ai-Qin Zhang:** Writing – review & editing, Supervision, Project administration, Funding acquisition, Conceptualization.

Declaration of competing interest

The authors declare that they have no known competing financial interests or personal relationships that could have appeared to influence the work reported in this paper.

Appendix A. Supplementary data

Supplementary data to this article can be found online at https://doi.org/10.1016/j.heliyon.2024.e29404.

References

[1] H. Sung, J. Ferlay, R.L. Siegel, M. Laversanne, I. Soerjomataram, A. Jemal, F. Bray, Global Cancer Statistics, GLOBOCAN estimates of incidence and mortality worldwide for 36 cancers in 185 countries, CA A Cancer J. Clin. 71 (3) (2020) 209–249.
[2] R.L. Siegel, K.D. Miller, N.S. Wagle, A. Jemal, Cancer statistics, CA A Cancer J. Clin. 73 (1) (2023) 17–48.
[3] Chen, P., Liu, Y., Wen, Y., & Zhou, C. Non-small cell lung cancer in China. Cancer Commun., 42(10), 937-970.
[4] Miller, M., & Hanna, N. Advances in systemic therapy for non-small cell lung cancer. BMJ, 375, n2363.
[5] Reck, M., Remon, J., & Hellmann, M. D. First-line immunotherapy for non-small-cell lung cancer. J. Clin. Oncol., 40(6), 586-597.
[6] Caushi, J. X., Zhang, J., Ji, Z., Vaghasia, A., Zhang, B., Hsiue, E. H., Mog, B. J., Hou, W., Justesen, S., Blosser, R., Tam, A., Anagnostou, V., Cottrell, T. R., Guo, H., Chan, H. Y., Singh, D., Thapa, S., Dykema, A. G., Burman, P., Choudhury, B., … Smith, K. N. Transcriptional programs of neoantigen-specific TIL in anti-PD-1-treated lung cancers. Nature, 596(7870), 126-132.
[7] Lopez de Rodas, M., Nagineni, V., Ravi, A., Datar, I. J., Mino-Kenudson, M., Corredor, G., Barrera, C., Behlman, L., Rimm, D. L., Herbst, R. S., Madabhushi, A., Riess, J. W., Velcheti, V., Hellmann, M. D., Gainor, J., & Schalper, K. A. Role of tumor infiltrating lymphocytes and spatial immune heterogeneity in sensitivity to PD-1 axis blockers in non-small cell lung cancer. J Immunother Cancer, 10(6), e004440.
[8] Mansouri, S., Heylmann, D., Stiewe, T., Kracht, M., & Savai, R. Cancer genome and tumor microenvironment: reciprocal crosstalk shapes lung cancer plasticity. Elife, 11, e79895.
[9] Dey, P., Kimmelman, A. C., & DePinho, R. A. Metabolic codependencies in the tumor microenvironment. Cancer Discov., 11(5), 1067-1081.
[10] Jhunjhunwala, S., Hammer, C., & Delamarre, L. Antigen presentation in cancer: insights into tumour immunogenicity and immune evasion. Nat. Rev. Cancer, 21 (5), 298-312.
[11] Tu, E., McGlinchey, K., Wang, J., Martin, P., Ching, S. L., Floc'h, N., Kurasawa, J., Starrett, J. H., Lazdun, Y., Wetzel, L., Nuttall, B., Ng, F. S., Coffman, K. T., Smith, P. D., Politi, K., Cooper, Z. A., & Streicher, K. Anti-PD-L1 and anti-CD73 combination therapy promotes T cell response to EGFR-mutated NSCLC. JCI insight, 7(3), e142843.
[12] Dolina, J. S., Van Braeckel-Budimir, N., Thomas, G. D., & Salek-Ardakani, S. CD8+ T cell exhaustion in cancer. Front. Immunol., 12, 715234.
[13] Martinez-Usatorre, A., Kadioglu, E., Boivin, G., Cianciaruso, C., Guichard, A., Torchia, B., Zangger, N., Nassiri, S., Keklikoglou, I., Schmittnaegel, M., Ries, C. H., Meylan, E., & De Palma, M. Overcoming microenvironmental resistance to PD-1 blockade in genetically engineered lung cancer models. Sci. Transl. Med., 13 (606), eabd1616.
[14] Zhou, B., Yuan, Y., Zhang, S., Guo, C., Li, X., Li, G., Xiong, W., & Zeng, Z. Intestinal flora and disease mutually shape the regional immune system in the intestinal tract. Front. Immunol., 11, 575.
[15] Zhao, Y., Liu, Y., Li, S., Peng, Z., Liu, X., Chen, J., & Zheng, X. Role of lung and gut microbiota on lung cancer pathogenesis. J. Cancer Res. Clin. Oncol., 147(8), 2177-2186.
[16] Roviello, G., Iannone, L. F., Bersanelli, M., Mini, E., & Catalano, M. The gut microbiome and efficacy of cancer immunotherapy. Pharmacol. Ther., 231, 107973.
[17] Tomioka, S., Seki, N., Sugiura, Y., Akiyama, M., Uchiyama, J., Yamaguchi, G., Yakabe, K., Ejima, R., Hattori, K., Kimizuka, T., Fujimura, Y., Sato, H., Gondo, M., Ozaki, S., Honme, Y., Suematsu, M., Kimura, I., Inohara, N., Núñez, G., Hase, K., … Kim, Y. G. Cooperative action of gut-microbiota-accessible carbohydrates improves host metabolic function. Cell Rep., 40(3), 111087.
[18] Mirzaei, R., Afaghi, A., Babakhani, S., Sohrabi, M. R., Hosseini-Fard, S. R., Babolhavaeji, K., Khani Ali Akbari, S., Yousefimashouf, R., & Karampoor, S. Role of microbiota-derived short-chain fatty acids in cancer development and prevention. Biomed. Pharmacother., 139:111619.
[19] Li, Z., Feiyue, Z., & Gaofeng, L. Traditional Chinese medicine and lung cancer–From theory to practice. Biomed. Pharmacother.. 137:111381.
[20] Su, X. L., Wang, J. W., Che, H., Wang, C. F., Jiang, H., Lei, X., Zhao, W., Kuang, H. X., & Wang, Q. H. Clinical application and mechanism of traditional Chinese medicine in treatment of lung cancer. Chin Med J (Engl), 133(24):2987-2997.
[21] Lili Wang, Lei Shi, Xiang Qian, L.I. Zhaodong, Effect of Qingfei mixture on immune function in patients with advanced NSCLC, J of New CHIN MED 50 (1) (2018) 105–107.
[22] Lili Wang, Lei Shi, Xiang Qian, Zhaodong Li, Effect of chemotherapy combined with Qingfei mixture on immune function in patients with non small cell lung cancer, Chin J of Gen Pract 15 (7) (2017) 1166–1168.
[23] Q. Li, X. Fu, X. Ge, F. Tao, P. Huang, M. Ge, H. Jin, Antitumor effects and related mechanisms of ethyl acetate extracts of polygonum perfoliatum L, Front. Oncol. 9 (2019) 578.
[24] Qian, X., Zhang, H. Y., Li, Q. L., Ma, G. J., Chen, Z., Ji, X. M., Li, C. Y., & Zhang, A. Q. Integrated microbiome, metabolome, and proteome analysis identifies a novel interplay among commensal bacteria, metabolites and candidate targets in non-small cell lung cancer. Clin. Transl. Med., 12(6):e947.
[25] Guo, Y., Yu, Y., Li, H., Ding, X., Li, X., Jing, X., Chen, J., Liu, G., Lin, Y., Jiang, C., Liu, Z., He, Y., Li, C., & Tian, Z. Inulin supplementation ameliorates hyperuricemia and modulates gut microbiota in Uox-knockout mice. Eur. J. Nutr., 60(4):2217-2230.
[26] Qian, X., Bi, Q. Y., Wang, Z. N., Han, F., Liu, L. M., Song, L. B., Li, C. Y., Zhang, A. Q., & Ji, X. M. Qingyihuaji Formula promotes apoptosis and autophagy through inhibition of MAPK/ERK and PI3K/Akt/mTOR signaling pathway on pancreatic cancer in vivo and in vitro. J. Ethnopharmacol., 307:116198.
[27] Luu, M., Riester, Z., Baldrich, A., Reichardt, N., Yuille, S., Busetti, A., Klein, M., Wempe, A., Leister, H., Raifer, H., Picard, F., Muhammad, K., Ohl, K., Romero, R., Fischer, F., Bauer, C. A., Huber, M., Gress, T. M., Lauth, M., Danhof, S., … Visekruna, A. Microbial short-chain fatty acids modulate CD8+ T cell responses and improve adoptive immunotherapy for cancer. Nat. Commun., 12(1):4077.
[28] I. Chattopadhyay, R. Gundamaraju, N.K. Jha, P.K. Gupta, A. Dey, C.C. Mandal, B.M. Ford, Interplay between dysbiosis of gut microbiome, lipid metabolism, and tumorigenesis: can gut dysbiosis stand as a prognostic marker in cancer? Dis. Markers (2022) 2941248.
[29] Lin, B., Wang, M., Gao, R., Ye, Z., Yu, Y., He, W., Qiao, N., Ma, Z., Ji, C., Shi, C., Zhou, X., Wang, Y., Zeng, F., Zhang, L., Gong, W., Cao, Z., Zhou, P., Melnikov, V., Ye, H., Li, Y., … Zhang, Y. Characteristics of gut microbiota in patients with GH-secreting pituitary adenoma. Microbiol. Spectr., 10(1):e0042521.
[30] Deng, Y., Ding, X., Huang, X., Yang, Y., & Chen, C. Metabolism of branched-chain amino acids revealed by transcriptome analysis in Vibrio alginolyticus. Mar. Genomics, 35:23-26.
[31] Louis, P., & Flint, H. J. Formation of propionate and butyrate by the human colonic microbiota. Environ. Microbiol., 19(1):29-41.
[32] Peterson, C. T., Rodionov, D. A., Osterman, A. L., & Peterson, S. N. B vitamins and their role in immune regulation and cancer. Nutrients, 12(11):3380.
[33] Cai, X., Li, H., Wang, M., Chu, E., Wei, N., Lin, J., Hu, Y., Dai, J., Chen, A., Zheng, H., Zhang, Q., Zhong, Y., Chang, R., Wu, S., Xiao, Y., & Liu, C. mTOR participates in the formation, maintenance, and function of memory CD8+T cells regulated by glycometabolism. Biochem. Pharmacol., 204:115197.
[34] El Hage, A., & Dormond, O. Combining mTOR inhibitors and T cell-based immunotherapies in cancer treatment. Cancers, 13(6):1359.
[35] Tian, Y., Zhai, X., Yan, W., Zhu, H., & Yu, J. Clinical outcomes of immune checkpoint blockades and the underlying immune escape mechanisms in squamous and adenocarcinoma NSCLC. Cancer Med.,10(1):3-14.
[36] Wei, S. C., Duffy, C. R., & Allison, J. P. Fundamental mechanisms of immune checkpoint blockade therapy. Cancer Discov., 8(9):1069-1086.
[37] Hu, X., Gu, Y., Zhao, S., Hua, S., & Jiang, Y. Elevated circulating CD4+CD25-Foxp3+ regulatory T cells in patients with nonsmall cell lung cancer. Cancer Biother. Radiopharm., 34(5):325-333.

[38] Iksen, Pothongsrisit, S., & Pongrakhananon, V. Targeting the PI3K/AKT/mTOR signaling pathway in lung cancer: an update regarding potential drugs and natural products. Molecules, 26(13):4100.
[39] Gremke, N., Polo, P., Dort, A., Schneikert, J., Elmshäuser, S., Brehm, C., Klingmüller, U., Schmitt, A., Reinhardt, H. C., Timofeev, O., Wanzel, M., & Stiewe, T. mTOR-mediated cancer drug resistance suppresses autophagy and generates a druggable metabolic vulnerability. Nat. Commun., 11(1):4684.
[40] Yan, C., Wu, D., Gan, L., Wang, J., Yang, W., & Xu, B. Significant metabolic alterations in non-small cell lung cancer patients by epidermal growth factor receptor-targeted therapy and PD-1/PD-L1 immunotherapy. Front. Pharmacol., 13:949745.
[41] Qin, X., Bi, L., Yang, W., He, Y., Gu, Y., Yang, Y., Gong, Y., Wang, Y., Yan, X., Xu, L., Xiao, H., & Jiao, L. Dysbiosis of the gut microbiome is associated with histopathology of lung cancer. Front. Microbiol., 13:918823.
[42] Matsushita, M., Fujita, K., Hayashi, T., Kayama, H., Motooka, D., Hase, H., Jingushi, K., Yamamichi, G., Yumiba, S., Tomiyama, E., Koh, Y., Hayashi, Y., Nakano, K., Wang, C., Ishizuya, Y., Kato, T., Hatano, K., Kawashima, A., Ujike, T., Uemura, M., … Nonomura, N. Gut microbiota-derived short-chain fatty acids promote prostate cancer growth via IGF1 signaling. Cancer Res., 81(15):4014-4026.
[43] Derosa, L., Routy, B., Thomas, A. M., Iebba, V., Zalcman, G., Friard, S., Mazieres, J., Audigier-Valette, C., Moro-Sibilot, D., Goldwasser, F., Silva, C. A. C., Terrisse, S., Bonvalet, M., Scherpereel, A., Pegliasco, H., Richard, C., Ghiringhelli, F., Elkrief, A., Desilets, A., Blanc-Durand, F., … Besse, B. Intestinal Akkermansia muciniphila predicts clinical response to PD-1 blockade in patients with advanced non-small-cell lung cancer. Nat. Med., 28(2):315-324.
[44] Niccolai, E., Baldi, S., Ricci, F., Russo, E., Nannini, G., Menicatti, M., Poli, G., Taddei, A., Bartolucci, G., Calabrò, A. S., Stingo, F. C., & Amedei, A. Evaluation and comparison of short chain fatty acids composition in gut diseases. World J. Gastroenterol., 25(36):5543-5558.
[45] He, J., Zhang, P., Shen, L., Niu, L., Tan, Y., Chen, L., Zhao, Y., Bai, L., Hao, X., Li, X., Zhang, S., & Zhu, L. Short-chain fatty acids and their association with signalling pathways in inflammation, glucose and lipid metabolism. Int. J. Mol. Sci., 21(17):6356.
[46] Lukovac, S., Belzer, C., Pellis, L., Keijser, B. J., de Vos, W. M., Montijn, R. C., & Roeselers, G. Differential modulation by Akkermansia muciniphila and Faecalibacterium prausnitzii of host peripheral lipid metabolism and histone acetylation in mouse gut organoids. mBio, 5(4):e01438-14.
[47] Luu, M., Weigand, K., Wedi, F., Breidenbend, C., Leister, H., Pautz, S., Adhikary, T., & Visekruna, A. Regulation of the effector function of CD8+ T cells by gut microbiota-derived metabolite butyrate. Sci. Rep., 8(1):14430.
[48] Qiu, J., Villa, M., Sanin, D. E., Buck, M. D., O'Sullivan, D., Ching, R., Matsushita, M., Grzes, K. M., Winkler, F., Chang, C. H., Curtis, J. D., Kyle, R. L., Van Teijlingen Bakker, N., Corrado, M., Haessler, F., Alfei, F., Edwards-Hicks, J., Maggi, L. B., Jr, Zehn, D., Egawa, T., … Pearce, E. L. Acetate promotes T cell effector function during glucose restriction. Cell Rep., 27(7):2063-2074.e5.
[49] Rauf, A., Khalil, A. A., Rahman, U. U., Khalid, A., Naz, S., Shariati, M. A., Rebezov, M., Urtecho, E. Z., de Albuquerque, R. D. D. G., Anwar, S., Alamri, A., Saini, R. K., & Rengasamy, K. R. R. Recent advances in the therapeutic application of short-chain fatty acids (SCFAs): an updated review. Crit. Rev. Food Sci. Nutr., 62 (22):6034-6054.